

# Square Attack: a query-efficient black-box adversarial attack via random search

Maksym Andriushchenko\*  
EPFL

maksym.andriushchenko@epfl.ch

Nicolas Flammarion  
EPFL

nicolas.flammarion@epfl.ch

Francesco Croce\*  
University of Tübingen

francesco.croce@uni-tuebingen.de

Matthias Hein  
University of Tübingen

matthias.hein@uni-tuebingen.de

## Abstract

We propose the Square Attack, a new score-based black-box  $l_2$  and  $l_\infty$  adversarial attack that does not rely on local gradient information and thus is not affected by gradient masking. The Square Attack is based on a randomized search scheme where we select localized square-shaped updates at random positions so that the  $l_\infty$ - or  $l_2$ -norm of the perturbation is approximately equal to the maximal budget at each step. Our method is algorithmically transparent, robust to the choice of hyperparameters, and is significantly more query efficient compared to the more complex state-of-the-art methods. In particular, on ImageNet we improve the average query efficiency for various deep networks by a factor of at least 2 and up to 7 compared to the recent state-of-the-art  $l_\infty$ -attack of Meunier et al. [34] while having a higher success rate. The Square Attack can even be competitive to gradient-based white-box attacks in terms of success rate. Moreover, we show its utility by breaking a recently proposed defense based on randomization. The code of our attack is available at <https://github.com/max-andr/square-attack>.

## 1. Introduction

Adversarial examples are of particular concern when it comes to applications of machine learning which are safety-critical. Many defenses against adversarial examples have been proposed [21, 53, 40, 5, 31, 1, 7] but with limited success, as new more powerful attacks could break many of them [11, 4, 35, 13, 54]. In particular, gradient obfuscation or masking [4, 35] is often the reason why seemingly robust models with respect to a certain type of attack turn out to be non-robust in the end. Gradient-based attacks are most often affected by this phenomenon (white-box attacks but also

\*Equal contribution.

Street sign  $\rightarrow$  parking meter

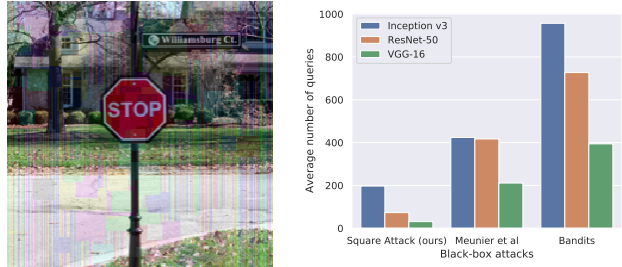


Figure 1. **Left:** Adversarial example generated for ResNet-50 by the Square Attack in the threat model  $\|\delta\|_\infty \leq 0.05$ . The  $l_\infty$  attack uses as initial perturbation stripes and then does random search using updates with squares. **Right:** avg. number of queries necessary for successful attacks on three ImageNet models for three score-based black-box attacks. The Square Attack outperforms all other attacks regarding query efficiency and success rate.

black-box attacks based on finite difference approximations [35]). Thus it is important to have attacks which are based on different principles. Black-box attacks have recently become more popular [36, 9, 46] as their attack strategies are quite different from the ones employed for adversarial training, where often PGD-type attacks [31] are used. However, a big problem at the moment is that these black-box attacks need to query the classifier too many times before they find adversarial examples and that their success rate is sometimes significantly lower than that of white-box attacks.

In this paper we propose the Square Attack, a simple score-based attack, that is we can query the probability distribution over the classes which the classifier predicts, but have no further access to the underlying model. The Square Attack is based on random search<sup>1</sup> [41, 43] which dates back to the 1960s. Random search has been successfully applied to reinforcement learning [32] where it came out to be competitive to gradient-based methods.

<sup>1</sup>Note that it is an iterative procedure which is different from a simple random sampling inside the feasible region.

The Square Attack requires significantly less queries compared to the state-of-the-art black-box methods in the score-based query model while outperforming them in terms of *success rate*, i.e. the percentage of successfully found adversarial examples. This is achieved by a combination of a particular initialization strategy and our square-shaped updates. We motivate why these updates are particularly suited to attack neural networks and provide also convergence guarantees for a variant of our method. In an extensive evaluation for different datasets (MNIST, CIFAR-10, ImageNet) and various normal and robust models, we show that the Square Attack outperforms recent state-of-the-art methods in the  $l_2$ - and  $l_\infty$ -threat model. We even break a recently proposed defense [30] based on randomization where the PGD attack yields a false impression of robustness while the model is actually not robust.

## 2. Related Work

We discuss black-box attacks for the threat model of perturbations in  $l_2$ - and  $l_\infty$ -ball as our method operates in these scenarios, although attacks for other norms, e.g.  $l_0$ , exist [36, 17] but are usually different algorithmically due to the specific geometry of the perturbation set.

**$l_2$  and  $l_\infty$  score-based attacks without extra knowledge.** Score-based black-box attacks have only access to the score predicted by a classifier for each class for a given input. Most of such attacks in the literature are based on gradient estimation through finite differences. In particular, the first papers in this direction [6, 25, 50] propose iterative attacks where at each step they approximate the gradient via sampling from some noise distribution around the point. While this general approach can be successful, it requires many queries of the classifier, particularly in high-dimensional input spaces like in image classification. Thus, improved techniques try to reduce the dimension of the search space via using the principal components of the data [6], searching for perturbations in the latent space of an auto-encoder [49] or using a low-dimensional noise distribution [26].

Other attacks exploit evolutionary strategies or random search. [3] use a genetic algorithm to generate adversarial examples and alleviate gradient masking as they successfully reduce the robust accuracy on randomization- and discretization-based defenses. The  $l_2$ -attack of [23] can be seen as a variant of random search where the search directions are chosen from some orthonormal basis and two candidate updates are tested at each iteration. However, their algorithm can have suboptimal query efficiency since at every step only very small (in  $l_2$  norm) modifications are added. Moreover, suboptimal modifications cannot be undone since they are orthogonal to each other.

A recent line of work has pursued black-box attacks which are based on the observation that successful adver-

sarial perturbations are attained at corners of the  $l_\infty$ -ball intersected with the image space  $[0, 1]^d$  [44, 34]. Searching only over the corners allows to apply discrete optimization techniques to generate adversarial attacks, significantly improving the query efficiency. Both [44] and [2] (with a few differences) divide the image according to some coarse grid, perform local search in this lower dimensional space allowing componentwise changes only of  $-\epsilon$  or  $\epsilon$ , then refine the grid and repeat iteratively the scheme. [2] motivate this procedure as an estimation of the gradient signs. Recently, [34] proposed several attacks based on different evolutionary algorithms, in the context of both discrete and continuous optimization, achieving state-of-the-art query efficiency for the  $l_\infty$ -norm. In order to reduce the dimensionality of the search space, they use the “tiling trick” of [26] where they divide the perturbation in a set of squares and modify the values in such squares with evolutionary algorithms. However, as in [26], both size and position of the squares are fixed at the beginning and not optimized. We note that despite the effectiveness of all these discrete optimization attacks for the  $l_\infty$ -norm, these approaches are not straightforward to adapt to the  $l_2$ -norm.

Finally, approaches based on Bayesian optimization exist, e.g. [45] combine it with the “tiling trick”, but show competitive performance only in a low-query regime.

**Different threat models.** While we focus on norm-bounded perturbations, some works aim at fooling perturbations with minimal  $l_p$ -norm (e.g. [49]) which often require more queries to be found. Thus, we do not compare to them, except for [23] which features competitive query efficiency while trying to have small perturbations.

In other cases the attacker has a level of knowledge of the classifier different from that here considered. A more restrictive scenario, considered by *decision-based* attacks [9, 14, 22, 10, 12], is where the attacker can query only the decision of the classifier, but not the predicted scores.

On the other hand, some works adopt more permissive threat models, e.g., the attacker already has a substitute model that is similar to the target one [39, 51, 15, 19]. In this setting, it can generate adversarial examples on the substitute model and then transfer them or, as in [51], perform a black-box gradient estimation attack in a subspace spanned by the gradients of substitute models. However, the gain in query efficiency given by such extra knowledge does not take into account the computational cost required to train such substitute models, particularly high on ImageNet-scale. Finally, some approaches use extra information about the data-generating distribution to train a model that directly predicts adversarial examples and then refines them with attacks based on gradient estimation [29].

### 3. Square Attack

In the following we recall the definitions of untargeted adversarial examples in the threat model where the perturbations are lying in some  $l_p$ -ball. Then, we present our black-box attacks for the  $l_\infty$ - and  $l_2$ -norms.

#### 3.1. Adversarial examples in the $l_p$ -threat model

Let  $f : [0, 1]^d \rightarrow \mathbb{R}^K$  be a classifier, where  $d$  is the input dimension,  $K$  the number of classes and  $f_k(x)$  is the predicted score that  $x$  belongs to class  $k$ . The classifier assigns class  $\arg \max_{k=1, \dots, K} f_k(x)$  to the input  $x$ .

The goal of an untargeted attack is to change the correctly predicted class  $y$  for the point  $x$ .  $\hat{x}$  is called an *adversarial example* with an  $l_p$ -norm bound of  $\epsilon$  for  $x$  if

$$\arg \max_{k=1, \dots, K} f_k(\hat{x}) \neq y \quad \text{and} \quad \|\hat{x} - x\|_p \leq \epsilon, \quad \hat{x} \in [0, 1]^d,$$

where we have added the additional constraint that  $\hat{x}$  is an image. The task of finding  $x_{\text{adv}}$  can be rephrased as solving the constrained optimization problem

$$\min_{\hat{x} \in [0, 1]^d} L(f(\hat{x}), y), \quad \text{s.t.} \quad \|\hat{x} - x\|_p \leq \epsilon \quad (1)$$

for a loss  $L$ . We use  $L(f(\hat{x}), y) = f_y(\hat{x}) - \max_{k \neq y} f_k(\hat{x})$  for the Square Attack. Note that  $L(f(\hat{x}), y) < 0$  implies that the decision for  $\hat{x}$  is different from  $y$ .

#### 3.2. General algorithmic scheme of Square Attack

Square Attack is based on random search (RS) which is a well known iterative technique in optimization introduced by Rastrigin in 1963 [41]. Let  $g$  be the function to minimize and  $\hat{x}^{(j)}$  the iterate at iteration  $j$ . RS samples a random update  $\delta$ . If  $g(\hat{x}^{(j)} + \delta) < g(\hat{x}^{(j)})$ , then  $\hat{x}^{(j+1)} = \hat{x}^{(j)} + \delta$ , else  $\hat{x}^{(j+1)} = \hat{x}^{(j)}$ . In other words, at each step the algorithm samples a random point close to the current iterate and checks if it improves the objective function. Despite its simplicity, RS performs well in many situations and is not dependent on gradient information from  $g$ .

Many variants of RS search have been introduced [33, 43, 42], which differ mainly in how the random perturbation is chosen at each iteration (the original scheme samples uniformly on a hypersphere of fixed radius). For our goal of crafting adversarial examples we come up with two sampling distributions specific to our problem: one for the  $l_\infty$  and one for the  $l_2$  attack (see Sec. 3.3 and Sec. 3.4), which we integrate in the classic RS procedure and are motivated by both how images are processed by networks with convolutional filters and the shape of the  $l_p$ -balls for different  $p$ .

Our scheme differs from classical random search by the fact the perturbations  $\hat{x} - x$  are constructed such that on every iteration they lie on the boundary of the  $l_\infty$ - or  $l_2$ -ball

---

#### Algorithm 1: The square attack via random search

---

**Input:** classifier  $f$ , point  $x \in \mathbb{R}^d$ , image size  $w$ , number of color channels  $c$ ,  $l_p$ -radius  $\epsilon$ , label  $y \in \{1, \dots, K\}$ , number of iterations  $N$

**Output:** approximate minimizer  $\hat{x} \in \mathbb{R}^d$  of (1)

- 1  $\hat{x} \leftarrow \text{init}(x)$ ,  $l^* \leftarrow L(f(x), y)$ ,  $i \leftarrow 1$
- 2 **while**  $i \leq N - 1$  **and**  $l^* > 0$  **do**
- 3      $h^{(i)} \leftarrow$  scheduled parameter which is the side length of the square to be modified
- 4      $\delta \sim P(\epsilon, h^{(i)}, w, c, \hat{x}, x) / *$  sample the update from some sampling distribution \*/
- 5      $\hat{x}_{\text{new}} \leftarrow \text{Project } \hat{x} + \delta \text{ onto } B_p(x, \epsilon) \cap [0, 1]^d$
- 6      $l_{\text{new}} \leftarrow L(f(\hat{x}_{\text{new}}), y)$
- 7     **if**  $l_{\text{new}} < l^*$  **then**  $\hat{x} \leftarrow \hat{x}_{\text{new}}$ ,  $l^* \leftarrow l_{\text{new}}$  ;
- 8      $i \leftarrow i + 1$
- 9 **end**

---

before projection onto the image domain  $[0, 1]^d$ . Thus we are using the perturbation budget almost optimally at each step. Moreover, the changes are localized on the image in the sense that, at each step, we modify just a small fraction of contiguous pixels shaped into **squares**. The overall scheme is presented in Algorithm 1. First, the algorithm picks the side length  $h^{(i)}$  of the square to be modified (step 3), which is decreasing according to an a priori fixed schedule. This is in analogy to the step-size reduction in gradient-based optimization method. Then in step 4 we sample a new update  $\delta$  and add it to the current iterate (step 5). If the resulting loss (obtained in step 6) is smaller than the loss so far, the change is accepted otherwise it is discarded. Since we are interested in a query efficient attack, the algorithm stops as soon as an adversarial example is found, that is  $l^* \leq 0$ . The overall time complexity of the algorithm is dominated by the evaluation of  $f(\hat{x}_{\text{new}})$ , thus the total running time of the algorithm is at most  $N$  forward passes of  $f$ , where  $N$  is the number of iterations of Square Attack. We plot the resulting adversarial examples in Figure 3.

**Size of the squares.** Given images with size  $w \times w$ , let  $p \in [0, 1]$  be the percentage of elements of  $x$  to be modified. The size  $h$  of the side of the squares we use (see step 3) is given by the closest positive integer to  $\sqrt{p \cdot w^2}$  (and  $h \geq 3$  for the  $l_2$  attack). Then, in practice the initial  $p$  is the only free parameter of our algorithm. With  $N = 10000$  iterations available, we halve the value of  $p$  at  $i \in \{10, 50, 200, 1000, 2000, 4000, 6000, 8000\}$  iterations. For different  $N$  we rescale the schedule accordingly.

---

**Algorithm 2:** Sampling distribution  $P$  for  $l_\infty$ -norm

---

**Input:** maximal norm  $\epsilon$ , window size  $h$ , image size  $w$ , color channels  $c$   
**Output:** New update  $\delta$

- 1  $\delta \leftarrow$  array of zeros of size  $w \times w \times c$
- 2 sample uniformly  $r, s \in \{0, \dots, w - h\} \subset \mathbb{N}$
- 3 **for**  $i = 1, \dots, c$  **do**
- 4      $\rho \leftarrow \text{Uniform}(\{-2\epsilon, 2\epsilon\})$
- 5      $\delta_{r+1:r+h, s+1:s+h, i} \leftarrow \rho \cdot \mathbb{1}_{h \times h}$
- 6 **end**

---

### 3.3. The $l_\infty$ Square Attack

*Initialization:* We initialize the perturbations with vertical stripes of width one since we found that convolutional networks are particularly sensitive to such perturbations. The color of each stripe is sampled from  $\text{Uniform}(\{-\epsilon, \epsilon\}^c)$ , where  $c$  is the number of color channels. Concurrently also [52] showed that neural networks are more generally vulnerable to *various* types of high frequency perturbations (although they evaluate perturbations of much larger magnitude than ours).

*Sampling distribution:* Similarly to [44] we observe that successful  $l_\infty$  perturbations usually have values  $\pm\epsilon$  in all the components (note that this does not hold perfectly due to the image constraints  $\hat{x} \in [0, 1]^d$ ). In particular, it holds

$$\hat{x}_i \in \{\max\{0, x_i - \epsilon\}, \min\{1, x_i + \epsilon\}\}.$$

Our sampling distribution  $P$  for the  $l_\infty$ -norm described in Algorithm 2 selects sparse updates of  $\hat{x}$  with  $\|\delta\|_0 = h \cdot h \cdot c$  where  $\delta \in \{-2\epsilon, 0, 2\epsilon\}^d$  and the non-zero elements are grouped to form a square. In this way, after the projection onto the  $l_\infty$ -ball of radius  $\epsilon$  (step 5 of Algorithm 1) all components  $i$  for which  $\epsilon \leq x_i \leq 1 - \epsilon$  satisfy  $\hat{x}_i \in \{x_i - \epsilon, x_i + \epsilon\}$ , that is differ from the original point  $x$  in each element either by  $\epsilon$  or  $-\epsilon$ . Thus  $\hat{x} - x$  is situated at one of the corners of the  $l_\infty$ -ball (modulo the components which are close to the boundary). Note that all projections are done by clipping. Moreover, we fix the elements of  $\delta$  belonging to the same color channel to have the same sign, since we observed that neural networks are particularly sensitive to such perturbations (see Figure 3).

### 3.4. The $l_2$ Square Attack

*Initialization:* The  $l_2$ -perturbation is initialized by generating a  $5 \times 5$  grid-like tiling by squares of the image, where the perturbation on each tile has the shape as described next in the sampling distribution. The resulting perturbation  $\hat{x} - x$  is rescaled to have  $l_2$ -norm  $\epsilon$  and the resulting  $\hat{x}$  is finally projected onto  $[0, 1]^d$  by clipping.

*Sampling distribution:* First, let us notice that the adversarial perturbations typically found for the  $l_2$ -norm tend to

---

**Algorithm 3:** Sampling distribution  $P$  for  $l_2$ -norm

---

**Input:** maximal norm  $\epsilon$ , window size  $h$ , image size  $w$ , number of color channels  $c$ , current image  $\hat{x}$ , original image  $x$   
**Output:** New update  $\delta$

- 1  $\nu \leftarrow \hat{x} - x$
- 2 sample uniformly  $r_1, s_1, r_2, s_2 \in \{0, \dots, w - h\}$
- 3 identify with
  - $W_1 := r_1 + 1 : r_1 + h, s_1 + 1 : s_1 + h$
  - $W_2 := r_2 + 1 : r_2 + h, s_2 + 1 : s_2 + h$

the indices of the elements in two square windows of side  $h$  subset of  $\nu$

- 4  $\epsilon_{\text{unused}}^2 \leftarrow \epsilon^2 - \|\nu\|_2^2$
- 5  $\eta^* \leftarrow \eta / \|\eta\|_2$  with  $\eta$  as in (2)
- 6 **for**  $i = 1, \dots, c$  **do**
- 7      $\rho \leftarrow \text{Uniform}(\{-1, 1\})$
- 8      $\nu_{\text{temp}} \leftarrow \rho \eta^* + \nu_{W_1, i} / \|\nu_{W_1, i}\|_2$
- 9      $\epsilon_{\text{avail}}^i \leftarrow \sqrt{\|\nu_{W_1 \cup W_2, i}\|_2^2 + \epsilon_{\text{unused}}^2 / c}$
- 10      $\nu_{W_2, i} \leftarrow 0$
- 11      $\nu_{W_1, i} \leftarrow (\nu_{\text{temp}} / \|\nu_{\text{temp}}\|_2) \epsilon_{\text{avail}}^i$
- 12 **end**
- 13  $\delta \leftarrow x + \nu - \hat{x}$

---

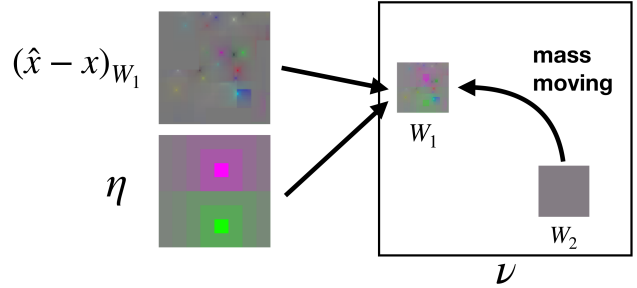


Figure 2. Perturbation at each iteration of the  $l_2$  attack.

be much more localized than those for the  $l_\infty$ -norm [48], in the sense that large changes are applied on some pixels of the original image, while many others are minimally modified. To mimic this feature we introduce a new update  $\eta$  which has two “centers” with large absolute value and opposite signs, while the other components have lower absolute values as one gets farther away from the centers, but never reaching zero (see Fig. 2 for one example with  $h = 8$  of the resulting update  $\eta$ ). In this way the modifications are localized and with high contrast between the different halves. More specifically, we define  $\eta^{(h_1, h_2)} \in \mathbb{R}^{h_1 \times h_2}$  (where we assume  $h_1 \geq h_2$ ), defined elementwise for every

$1 \leq r \leq h_1, 1 \leq s \leq h_2$  as

$$\eta_{r,s}^{(h_1,h_2)} = \sum_{k=0}^{M(r,s)} \frac{1}{(n+1-k)^2}, \quad \text{with } n = \left\lfloor \frac{h_1}{2} \right\rfloor$$

and  $M(r,s) = n - \max\{|r - \lfloor \frac{h_1}{2} \rfloor - 1|, |s - \lfloor \frac{h_2}{2} \rfloor - 1|\}$ . The intermediate square update  $\eta \in \mathbb{R}^{h \times h}$  is then selected uniformly at random from either

$$\eta = \left( \eta^{(h,k)}, -\eta^{(h,h-k)} \right), \quad \text{with } k = \lfloor h/2 \rfloor, \quad (2)$$

or its transpose (corresponding to a rotation of  $90^\circ$ ).

Second, unlike  $l_\infty$ -constraints,  $l_2$ -constraints do not allow to modify each component independently from the others as the overall norm must be kept smaller than  $\epsilon$ . Therefore, if we want to modify a perturbation  $\hat{x} - x$  of norm  $\epsilon$  through localized changes while staying on the hypersphere, we have to “move the mass” of  $\hat{x} - x$  from one location to another.

Thus our scheme consists in randomly selecting two square windows of the perturbation  $\nu = \hat{x} - x$ , namely  $\nu_{W_1}$  and  $\nu_{W_2}$ , setting  $\nu_{W_2} = 0$  and using the budget of  $\|\nu_{W_2}\|_2$  to increase the total perturbation of  $\nu_{W_1}$ . Note that the perturbation of  $W_1$  is then a combination of the existing perturbation plus the new generated  $\eta$ . We report the details of this scheme in Algorithm 3 where step 4 allows to utilize the budget of  $l_2$ -norm lost after the projection onto  $[0, 1]^d$ . The update  $\delta$  output by the algorithm is such that the next iterate  $\hat{x}_{\text{new}} = \hat{x} + \delta$  (before projection onto  $[0, 1]^d$  by clipping) belongs to the hypersphere  $B_2(x, \epsilon)$  as stated in the following proposition.

**Proposition 3.1** *Let  $\delta$  be the output of Algorithm 3. Then  $\|\hat{x} + \delta - x\|_2 = \epsilon$ .*

## 4. Theoretical justification of the algorithm

In this section, we provide high-level theoretical intuition why the choices done in Square Attack are justified. We analyze the  $l_\infty$ -version as the  $l_2$ -version is significantly harder to analyze.

### 4.1. Convergence analysis of Random Search

First, we want to study the convergence of the random search algorithm an  $L$ -smooth function  $g$  (such as neural networks with activation functions like softplus, swish, ELU, etc) on the whole space  $\mathbb{R}^d$  (without projection<sup>2</sup>) under the following assumptions on the update  $\delta_t$  drawn from the sampling distribution  $P_t$ :

$$\mathbb{E}\|\delta_t\|_2^2 \leq \gamma_t^2 C \quad \text{and} \quad \mathbb{E}|\langle \delta_t, v \rangle| \geq \tilde{C} \gamma_t \|v\|_2, \quad \forall v \in \mathbb{R}^d. \quad (3)$$

<sup>2</sup> Nonconvex constrained optimization under noisy oracles is notoriously more difficult [18]

where  $\gamma_t$  is the step size at iteration  $t$ , and  $C, \tilde{C}$  are some positive constants. We obtain the following result which is similar to existing convergence rates for zeroth-order methods [37, 38, 20]:

**Proposition 4.1** *Suppose that  $\mathbb{E}[\delta_t] = 0$  and Assumption 3 holds. Then for step-sizes  $\gamma_t = \gamma/\sqrt{T}$ , we have*

$$\min_{t=0,\dots,T} \mathbb{E}\|\nabla g(x_t)\|_2 \leq \frac{2}{\gamma \tilde{C} \sqrt{T}} \left( g(x_0) - \mathbb{E}g(x_{T+1}) + \frac{\gamma^2 CL}{2} \right).$$

This basically shows for  $T$  large enough one can make the gradient arbitrary small, meaning that the random search algorithm converges to a critical point of  $g$  (one cannot hope for much stronger results in non-convex optimization without stronger conditions).

Unfortunately, the second part of Assumption 3 does not directly hold for our sampling distribution  $P$  for the  $l_\infty$ -norm (see Sup. A.3). However, it holds for a similar sampling distribution  $P^{\text{multiple}}$  where each component of the update  $\delta$  is drawn uniformly at random from  $\{-2\epsilon, 2\epsilon\}$ . We show using the Khintchine inequality [24] (see Sup. A.4)

$$\mathbb{E}\|\delta_t\|_2^2 \leq 4c\epsilon^2 h^2 \quad \text{and} \quad \mathbb{E}|\langle \delta_t, v \rangle| \geq \frac{\sqrt{2}c\epsilon h^2}{d} \|v\|_2, \quad \forall v \in \mathbb{R}^d.$$

We note that the size of the window acts as a step-size here. In our experiments, however, the componentwise random update scheme was significantly worse. We provide arguments why this is the case in the supplementary material.

### 4.2. Why squares?

Previous works [44, 34] build their  $l_\infty$  attacks by iteratively adding square modifications. Likewise we change square-shaped regions of the image for both our  $l_\infty$  and  $l_2$  attacks—with the difference that we can sample any square subset of the input, while the grid of the possible squares is fixed in [44, 34]. This leads naturally to ask why squares are superior to other shapes, e.g., rectangles.

Let us consider the  $l_\infty$  threat model, with bound  $\epsilon$ , input space  $\mathbb{R}^{d \times d}$  and a convolutional filter  $w \in \mathbb{R}^{s \times s}$  with entries unknown to the attacker. Let  $\delta \in \mathbb{R}^{d \times d}$  be the sparse update with  $\|\delta\|_0 = k \geq s^2$  and  $\|\delta\|_\infty \leq \epsilon$ . We denote by  $S(a, b)$  the index set of the rectangular support of  $\delta$  with  $|S(a, b)| = k$  and shape  $a \times b$ . We want to give intuition why sparse square-shaped updates are superior to rectangular ones in the sense of reaching maximal change in the activation of the first convolutional layer.

Let  $z = \delta * w \in \mathbb{R}^{d \times d}$  denote the output of the convolutional layer for the update  $\delta$ . The  $l_\infty$ -norm of  $z$  is the maximal componentwise change of the convolutional layer:

$$\begin{aligned} \|z\|_\infty &= \max_{u,v} |z_{u,v}| = \max_{u,v} \left| \sum_{i,j=1}^s \delta_{u-\lfloor \frac{s}{2} \rfloor+i, v-\lfloor \frac{s}{2} \rfloor+j} \cdot w_{i,j} \right| \\ &\leq \max_{u,v} \epsilon \sum_{i,j} |w_{i,j}| \mathbb{1}_{(u-\lfloor \frac{s}{2} \rfloor+i, v-\lfloor \frac{s}{2} \rfloor+j) \in S(a,b)} \end{aligned}$$

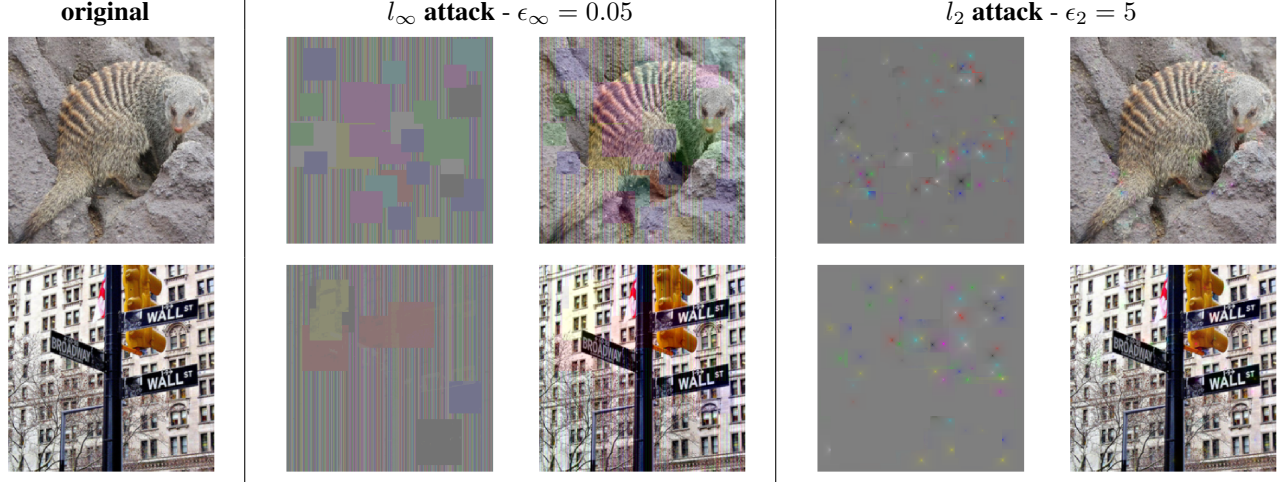


Figure 3. Visualization of the adversarial perturbations and examples found by the  $l_\infty$  and  $l_2$  versions of the Square Attack on ResNet-50.

with the convention that elements with indices exceeding the size of the matrix are set to zero. Note that the indicator function attains 1 only for the non-zero elements of  $\delta$  involved in the convolution to get  $z_{u,v}$ . Thus, in order to have the largest upper bound possible on  $|z_{u,v}|$ , for some  $(u, v)$ , we need the largest amount possible of components of  $\delta$  with indices in

$$C(u, v) = \left\{ \left( u - \lfloor \frac{s}{2} \rfloor + i, v - \lfloor \frac{s}{2} \rfloor + j \right) : i, j = 1, \dots, s \right\}$$

to be non-zero (that is in  $S(a, b)$ ).

Therefore, it is desirable to have  $S(a, b)$  shaped so to maximize the number  $N$  of squares of side length  $s$ , i.e. the shape of the filter  $w$ , which fit into the rectangle  $a \times b$ , i.e. the shape of the subset of non-zero elements of  $\delta$ . Let  $\mathcal{F}$  be the family of the objects that can be defined as the union of axis-aligned rectangles with vertices on  $\mathbb{N}^2$ , and  $\mathcal{G} \subset \mathcal{F}$  the squares of  $\mathcal{F}$  of shape  $s \times s$  with  $s \geq 2$ . We have the following proposition:

**Proposition 4.2** *Among the elements of  $\mathcal{F}$  with area  $k \geq s^2$ , those which contain the largest number of elements of  $\mathcal{G}$  have*

$$N^* = (a - s + 1)(b - s + 1) + (r - s + 1)^+ \quad (4)$$

of them, with  $a = \lfloor \sqrt{k} \rfloor$ ,  $b = \lfloor \frac{k}{a} \rfloor$ ,  $r = k - ab$  and  $z^+ = \max\{z, 0\}$ .

This proposition states that, if we can select only  $k$  elements of  $\delta$  to modify, then shaping them to form (approximately) a square allows to maximize the number of pairs  $(u, v)$  for which  $|S(a, b) \cap C(u, v)| = s^2$ . Note that if  $k = l^2$  then  $a = b = l$  thus it is exactly a square which is optimal to maximize the overlap of convolutional filters and our update of the perturbation.

## 5. Experiments

In this section we show the effectiveness of the Square Attack. First, we follow the standard setup [26, 34] of comparing black-box attacks for three models on ImageNet in terms of success rate and query efficiency for the  $l_\infty$  and  $l_2$  threat models (see Sec. 5.1). Our Square Attack outperforms the competitors in all these metrics, often by a large margin. Our proposed attack also has a higher success rate in the low query regime (up to 200 queries) which we cover in Sup. E.1. Second, we show our attack succeeds in fooling particular models where white-box PGD attacks or other state-of-the-art black box attacks suggest that they are seemingly robust (Sec. 5.2). Therefore, we believe that due its effectiveness and simplicity the Square Attack should become a standard attack in order to evaluate the robustness of neural networks. Finally, in the supplementary material we provide more information about the experimental details in Sup. B, we do additional experiments and analysis regarding the transferability of the adversarial perturbations produced by our attack in Sup. C, an ablation study of the different components of our scheme in Sup. D, additional experimental results in Sup. E, and stability of the attack under different random seeds in Sup. F. The code of the attack and experiments is available at <https://github.com/max-andr/square-attack>.

### 5.1. Evaluation on ImageNet

We compare the Square Attack to state-of-the-art score-based black-box attacks (without any extra information, e.g. surrogate models) for  $l_\infty$  [27, 44, 2, 34] and for  $l_2$  [27, 23]. Additionally, we provide a comparison to [45] in the low-query regime in Sup. E.1. We do not compare to [3] since the median number of queries they report is an order of magnitude larger than the methods we consider.

Norm	Attack	Failure rate			Avg. queries			Median queries		
		I	R	V	I	R	V	I	R	V
$l_\infty$	Bandits [26]	3.4%	1.4%	2.0%	957	727	394	218	136	36
	Parsimonious [44]	1.5%	-	-	722	-	-	237	-	-
	Sign bits [2]	2.0%	-	-	579	-	-	-	-	-
	DFO <sub>c</sub> – CMA, 50 tiles [34]	0.8%	<b>0.0%</b>	0.1%	630	270	219	259	143	107
	DFO <sub>d</sub> – Diag. CMA, 30 tiles [34]	2.3%	1.2%	0.5%	424	417	211	<b>20</b>	20	2
	<b>Square Attack (ours)</b>	<b>0.3%</b>	<b>0.0%</b>	<b>0.0%</b>	<b>197</b>	<b>73</b>	<b>31</b>	24	<b>11</b>	<b>1</b>
$l_2$	Bandits [26]	9.8%	6.8%	10.2%	1486	939	511	660	392	196
	SimBA-DCT [23]	35.5%	12.7%	7.9%	<b>651</b>	<b>582</b>	452	564	467	360
	<b>Square Attack (ours)</b>	<b>7.1%</b>	<b>0.7%</b>	<b>0.8%</b>	1100	616	<b>377</b>	<b>385</b>	<b>170</b>	<b>109</b>

Table 1. Results on ImageNet with a limit of 10,000 queries. For the  $l_\infty$  attacks we set the norm bound  $\epsilon = 0.05$  and for the  $l_2$  attacks  $\epsilon = 5$ . Models: normally trained **I**: Inception v3, **R**: ResNet-50, **V**: VGG-16-BN. The Square Attack outperforms for both threat models all other methods in terms of success rate and query efficiency. The missing entries correspond to the results taken from the papers where some models or statistics were not reported.

Attack	Avg. queries			Median queries		
	I	R	V	I	R	V
Bandits [26]	536	635	398	368	314	177
SimBA-DCT [23]	647	563	421	552	446	332
<b>Square Attack</b>	<b>352</b>	<b>287</b>	<b>217</b>	<b>181</b>	<b>116</b>	<b>80</b>

Table 2. Query statistics for  $l_2$  attacks computed for the points for which all three attacks are successful for fair comparison.

We run all the attacks on three pretrained models in PyTorch (for some attacks we report the numbers from their papers), namely Inception v3, ResNet-50, VGG-16-BN, using 1,000 images from the ImageNet validation set. As it is standard in the literature, we give a budget of 10,000 queries per point to find an adversarial perturbation of  $l_p$ -norm smaller than or equal to  $\epsilon$ . We report *average* and *median* number of queries each attack needs to craft an adversarial example, together with the failure rate. All statistics are only computed for originally correctly classified points and the query statistics is additionally only computed for successful attacks.

One can see how the Square Attack, despite its simplicity, achieves in all the cases (models and norms considered) the **lowest failure rate**, which is lower than 1% everywhere except for the  $l_2$  attack on Inception v3. Moreover, in almost all cases it requires **fewer queries** than the competitors for a successful attack. In fact, the  $l_\infty$  attack requires on average between 2 and 7 times smaller number of queries and the  $l_2$  attack improves query complexity by at least a factor of 1.5 and up to 2.2 on all the models when evaluated only on the points where all the attacks are successful (see Table 2). We highlight that we set the only hyperparameter of our attack,  $p$ , which regulates the size of the squares, for all the models as  $p = 0.05$  for  $l_\infty$ - and  $p = 0.1$  for  $l_2$ -perturbations.

**$l_\infty$  attacks.** We compare the Square Attack to the following black-box attacks: Bandits [27], Parsimonious [44], Sign bits [2], DFO<sub>c</sub> and DFO<sub>d</sub> [34]. We run Bandits using their publicly available code, with their suggested hyperparameters. For Sign bits and DFO there is no official implementation, so the statistics about their performance are taken directly from the respective papers. [44] provide code for the Parsimonious Attack but it is incompatible with the PyTorch models used for the other attacks, so we show only the results on Inception v3 reported in the original paper.

In Table 1 we report the comparison of the  $l_\infty$  attacks on ImageNet (we allow maximal perturbations of size  $\epsilon = 0.05$ ). First of all, the Square Attack always has the lowest failure rate, notably achieving 0.0% in 2 out of 3 cases, and the smallest number of queries in average needed to find adversarial examples, improving up to almost 7 times upon the best of the other methods (31 vs 211 queries on VGG-16-BN). Interestingly, our attack has median equal 1 on VGG-16-BN, meaning that the initialization with stripes is particularly effective for this model.

The closest competitor among the  $l_\infty$ -attacks is the CMA method of [34]. Note that their method with failure rates closer to our attack, DFO<sub>c</sub> – CMA, has much worse query efficiency – in terms of both the mean number of queries and, particularly, the median. Although DFO<sub>d</sub> requires a median number of queries comparable to our method, it needs much more queries on average, and also has significantly higher failure rate. Finally, we note that the full-covariance CMA algorithm of [34] has a computational complexity quadratic in the dimension of the input space, which is an expensive operation given high-dimensional inputs such as images. On the contrary, our method is more efficient since it has only operations of linear complexity.

**$l_2$  attacks.** We compare our attack to Bandits [26] and SimBA [23]. Note that we do not consider the  $l_2$  version of Sign Bits [2] since it is not as competitive as in the  $l_\infty$

scenario, and in particular worse than Bandits on ImageNet. We use the code of Bandits with their standard parameters. We consider the SimBA attack successful in the same setting as all other attacks, i.e. when the  $l_2$ -norm of the adversarial perturbation is smaller than  $\epsilon$  (we set  $\epsilon = 5$ ). We use the code from the paper repository with the parameters suggested by the authors for each of the three models.

As Table 1 shows, the Square Attack outperforms by a large margin the other methods in terms of failure rate. In Table 1 the average and median queries required are computed for each attack on the points where it was successful, which means that for different methods different points are used. In this setting, our attack achieves the lowest median number of queries for all the models and the lowest average one for VGG-16-BN. However, since it has a significantly lower failure rate, the statistics of the Square Attack are biased by the “hard” cases where the competitors fail. We recompute the same statistics about query consumption considering only the points where all the attacks are successful (Table 2). In this case, our method improves by at least 1.5 times the mean and by at least 2 times the median number of queries used to find adversarial perturbations for the same images.

## 5.2. Performance on Challenging Tasks

In this paragraph we show that the Square Attack performs very well on problems which are challenging for white-box and other black-box attacks such as Bandits [26] and SimBA [23] (we do not evaluate [34, 2] because they do not provide the code of their methods). In particular, we break a recently proposed randomized defense and show that the Square Attack works well where PGD but also other black-box methods suffer from gradient masking. In the following, we use for evaluation *robust accuracy*, which is defined as the worst-case accuracy of a classifier when an attack is allowed to perturb each input in an  $l_p$ -ball of a given radius  $\epsilon$ .

**Breaking the post-averaging defense.** We investigate whether the  $l_\infty$  robustness claims of [30] hold (as reported at <https://www.robust-ml.org/preprints/>). Their defense method is a randomized averaging method similar in spirit to [16]. The difference is that [30] sample from the surfaces of several  $d$ -dimensional spheres instead of a Gaussian, and they do not derive any robustness certificates, but rather measure robustness by the PGD attack. We use the hyperparameters specified in their code (K=15, R=6 on CIFAR-10 and K=15, R=30 on Imagenet). We show in Table 3 that the proposed defense can be broken by the  $l_\infty$  Square Attack, which is able to reduce the robust accuracy suggested by the evaluation with PGD from 88.4% to 15.8% on CIFAR-10 and from 76.1% to 0.4% on ImageNet.

$\epsilon_\infty$	Dataset	Robust accuracy		
		Clean	PGD	Square Attack
8/255	CIFAR-10	92.6%	88.4%	<b>15.8%</b>
	ImageNet	77.3%	76.1%	<b>0.4%</b>

Table 3.  $l_\infty$  robustness of the post-averaging randomized defense [30]. The Square Attack is able to defeat this defense.

### Attacking Clean Logit Pairing and Logit Squeezing.

These two defenses wrt  $l_\infty$  proposed in [28] have been broken. However, [35] needed up to 10k restarts of PGD attack which is computationally prohibitive. Using the publicly available models from [35], we run the Square Attack with  $p = 0.3$  and 20k query limit and report the results in Table 4. We obtain robust accuracy similar to PGD<sub>R</sub> in most cases, but with a *single run*, i.e. without additional restarts. At the same time, Bandits show considerably worse results than the Square Attack, although they still perform better than PGD<sub>I</sub> on the CLP<sub>MNIST</sub> and LSQ<sub>MNIST</sub> models.

$\epsilon_\infty$	Model	Robust accuracy			
		PGD <sub>I</sub>	PGD <sub>R</sub>	Bandits	Square
0.3	CLP <sub>MNIST</sub>	62.4%	<b>4.1%</b>	33.3%	6.1%
	LSQ <sub>MNIST</sub>	70.6%	5.0%	37.3%	<b>2.6%</b>
16/255	CLP <sub>CIFAR</sub>	2.8%	<b>0.0%</b>	14.3%	<b>0.2%</b>
	LSQ <sub>CIFAR</sub>	27.0%	<b>1.7%</b>	27.7%	7.2%

Table 4.  $l_\infty$  robustness of Clean Logit Pairing (CLP), Logit Squeezing (LSQ) [28]. The Square Attack with 20k queries is competitive to PGD (white-box) with many restarts (R=10,000 and R=100 on MNIST and CIFAR-10 respectively) and more effective than Bandits (black-box).

**Adversarial training.** Adversarial training [31] is one of the state-of-the-art techniques to train robust models. We attack the  $l_\infty$  adversarially trained models on MNIST and CIFAR-10 with  $l_\infty$  attacks and present the results (on 1000 points) in Table 5. With our simple random search algorithm we are able to get a robust accuracy of 87.1%. The Square Attack with 20k queries is competitive to PGD with many restarts and more effective than Bandits.

$\epsilon_\infty$	Model	Robust accuracy			
		PGD <sub>I</sub>	PGD <sub>R</sub>	Bandits	Square
0.3	AT <sub>MNIST</sub>	92.5%	89.6%	89.4%	<b>87.1%</b>
8/255	AT <sub>CIFAR</sub>	47.0%	<b>45.2%</b>	52.7%	46.1%

Table 5.  $l_\infty$  robustness of the  $l_\infty$  adversarially trained models of [31].  $R = 50$  and  $R = 10$  are the random restarts of PGD on MNIST and CIFAR-10 respectively.

In Table 6 we report the robust accuracy at different thresholds  $\epsilon$  of the  $l_\infty$  adversarially trained models on MNIST of [31] for the  $l_2$ -threat model. It is known that the PGD attack fails to successfully reduce the robust accuracy



$\epsilon_2$	Robust accuracy					
	PGD <sub>1</sub>	PGD <sub>10</sub>	PGD <sub>100</sub>	Bandits	SimBA	Square
1.0	91.5%	90.6%	89.3%	91.7%	97.6%	<b>89.2%</b>
1.5	86.1%	80.8%	76.7%	87.6%	94.1%	<b>60.8%</b>
2.0	79.6%	67.4%	59.8%	80.1%	87.6%	<b>16.7%</b>
2.5	69.2%	51.3%	36.0%	32.4%	75.8%	<b>2.4%</b>
3.0	57.6%	29.8%	12.7%	12.5%	58.1%	<b>0.6%</b>

Table 6.  $l_2$  robustness of the  $l_\infty$ -adversarially trained models of [31] at different thresholds  $\epsilon$ . PGD is shown with 1, 10, 100 random restarts. The black-box attacks are given a 10k queries budget (see the supplement for details).

for this threat model since it suffers from gradient masking [47]. Strikingly, in contrast to PGD and other black-box attacks we consider, our Square Attack does not suffer by gradient masking and yields robust accuracy close to zero for  $\epsilon = 2.5$ . This is obtained with only a single run compared to the multiple random restarts used for PGD.

## 6. Conclusion

We have presented the randomized score-based Square Attack which outperforms the state-of-the-art both in terms of query-efficiency and success rate and have used it to break a recently proposed defense where the PGD-attack overestimates robustness massively. We have also provided theoretical background why the Square Attack works well. In future work it would be interesting to use the Square Attack to explore the set of adversarial examples for a sensitivity analysis of neural networks.

## Acknowledgements

We are very grateful to Laurent Meunier and Satya Narayan Shukla for providing the data for Figure 5. M.A. also thanks Apostolos Modas for fruitful discussions.

M.H. and F.C. acknowledge support from the BMBF through the Tübingen AI Center (FKZ: 01IS18039A), the DFG TRR 248, project number 389792660 and the DFG Excellence Cluster Machine Learning - New Perspectives for Science, EXC 2064/1, project number 390727645.

## References

- [1] N. Akhtar and A. Mian. Threat of adversarial attacks on deep learning in computer vision: A survey. *IEEE Access*, 6:14410–14430, 2018.
- [2] A. Al-Dujaili and U.-M. O’Reilly. There are no bit parts for sign bits in black-box attacks. *ArXiv*, abs/1902.06894, 2019.
- [3] M. Alzantot, Y. Sharma, S. Chakraborty, and M. Srivastava. Genattack: practical black-box attacks with gradient-free optimization. *Genetic and Evolutionary Computation Conference (GECCO)*, 2019.
- [4] A. Athalye, N. Carlini, and D. A. Wagner. Obfuscated gradients give a false sense of security: Circumventing defenses to adversarial examples. In *ICML*, 2018.
- [5] O. Bastani, Y. Ioannou, L. Lampropoulos, D. Vytiniotis, A. Nori, and A. Criminisi. Measuring neural net robustness with constraints. In *NeurIPS*, 2016.
- [6] A. N. Bhagoji, W. He, B. Li, and D. Song. Practical black-box attacks on deep neural networks using efficient query mechanisms. In *ECCV*, 2018.
- [7] B. Biggio and F. Roli. Wild patterns: Ten years after the rise of adversarial machine learning. *Pattern Recognition*, 84:317–331, 2018.
- [8] S. Boyd and L. Vandenberghe. *Convex Optimization*. Cambridge University Press, Cambridge, 2004.
- [9] W. Brendel, J. Rauber, and M. Bethge. Decision-based adversarial attacks: Reliable attacks against black-box machine learning models. *ICLR*, 2018.
- [10] T. Brunner, F. Diehl, M. T. Le, and A. Knoll. Guessing smart: biased sampling for efficient black-box adversarial attacks. *ICCV*, 2019.
- [11] N. Carlini and D. Wagner. Adversarial examples are not easily detected: Bypassing ten detection methods. In *ACM Workshop on Artificial Intelligence and Security*, 2017.
- [12] J. Chen, M. I. Jordan, and Wainwright M. J. Hop-SkipJumpAttack: a query-efficient decision-based attack. *arXiv preprint arXiv:1904.02144*, 2019.
- [13] P. Chen, Y. Sharma, H. Zhang, J. Yi, and C. Hsieh. Ead: Elastic-net attacks to deep neural networks via adversarial examples. In *AAAI*, 2018.
- [14] M. Cheng, T. Le, P.-Y. Chen, J. Yi, H. Zhang, and C.-J. Hsieh. Query-efficient hard-label black-box attack: An optimization-based approach. *arXiv preprint arXiv:1807.04457*, 2018.
- [15] S. Cheng, Y. Dong, T. Pang, H. Su, and J. Zhu. Improving black-box adversarial attacks with a transfer-based prior. In *NeurIPS*, 2019.
- [16] J. M. Cohen, E. Rosenfeld, and Z. Kolter. Certified adversarial robustness via randomized smoothing. *ICML*, 2019.
- [17] F. Croce and M. Hein. Sparse and imperceptible adversarial attacks. In *ICCV*, 2019.
- [18] D. Davis and D. Drusvyatskiy. Stochastic model-based minimization of weakly convex functions. *SIAM Journal on Optimization*, 29(1):207–239, 2019.
- [19] J. Du, H. Zhang, J. T. Zhou, Y. Yang, and J. Feng. Query-efficient meta attack to deep neural networks. *arXiv preprint arXiv:1906.02398*, 2019.
- [20] J. Duchi, M. Jordan, M. Wainwright, and A. Wibisono. Optimal rates for zero-order convex optimization: The power of two function evaluations. *IEEE Transactions on Information Theory*, 61(5):2788–2806, 2015.
- [21] S. Gu and L. Rigazio. Towards deep neural network architectures robust to adversarial examples. In *ICLR Workshop*, 2015.
- [22] C. Guo, J. S. Frank, and K. Q. Weinberger. Low frequency adversarial perturbation. *UAI*, 2019.
- [23] C. Guo, J. R. Gardner, Y. You, A. G. Wilson, and K. Q. Weinberger. Simple black-box adversarial attacks. In *ICML*, 2019.
- [24] U. Haagerup. The best constants in the Khintchine inequality. *Studia Math.*, 70(3):231–283 (1982), 1981.

- [25] A. Ilyas, L. Engstrom, A. Athalye, and J. Lin. Black-box adversarial attacks with limited queries and information. *ICML*, 2018.
- [26] A. Ilyas, L. Engstrom, and A. Madry. Prior convictions: Black-box adversarial attacks with bandits and priors. *ICLR*, 2019.
- [27] A. Ilyas, S. Santurkar, D. Tsipras, L. Engstrom, B. Tran, and A. Madry. Adversarial examples are not bugs, they are features. *NeurIPS*, 2019.
- [28] H. Kannan, A. Kurakin, and I. Goodfellow. Adversarial logit pairing. *arXiv preprint arXiv:1803.06373*, 2018.
- [29] Y. Li, L. Li, L. Wang, T. Zhang, and B. Gong. Nattack: Learning the distributions of adversarial examples for an improved black-box attack on deep neural networks. *ICML*, 2019.
- [30] Y. Lin, H. Jiang, and H. Jiang. Bandlimiting neural networks against adversarial attacks. *arXiv preprint arXiv:1905.12797*, 2019.
- [31] A. Madry, A. Makelov, L. Schmidt, D. Tsipras, and A. Vladu. Towards deep learning models resistant to adversarial attacks. *ICLR*, 2018.
- [32] H. Mania, A. Guy, and B. Recht. Simple random search of static linear policies is competitive for reinforcement learning. In *NeurIPS*, 2018.
- [33] J. Matyas. Random optimization. *Automation and Remote control*, 26(2):246–253, 1965.
- [34] L. Meunier, J. Atif, and O. Teytaud. Yet another but more efficient black-box adversarial attack: tiling and evolution strategies. *arXiv preprint, arXiv:1910.02244*, 2019.
- [35] M. Mosbach, M. Andriushchenko, T. Trost, M. Hein, and D. Klakow. Logit pairing methods can fool gradient-based attacks. In *NeurIPS 2018 Workshop on Security in Machine Learning*, 2018.
- [36] N. Narodytska and S. Kasiviswanathan. Simple black-box adversarial attacks on deep neural networks. In *CVPR Workshops*, 2017.
- [37] A. S. Nemirovsky and D. B. Yudin. *Problem Complexity and Method Efficiency in Optimization*. Wiley-Interscience Series in Discrete Mathematics. John Wiley & Sons, 1983.
- [38] Y. Nesterov and V. Spokoiny. Random gradient-free minimization of convex functions. *Foundations of Computational Mathematics*, 17(2):527–566, 2017.
- [39] N. Papernot, P. McDaniel, and I. Goodfellow. Transferability in machine learning: from phenomena to black-box attacks using adversarial samples. *arXiv preprint arXiv:1605.07277*, 2016.
- [40] N. Papernot, P. McDonald, X. Wu, S. Jha, and A. Swami. Distillation as a defense to adversarial perturbations against deep networks. In *IEEE Symposium on Security & Privacy*, 2016.
- [41] L. Rastrigin. The convergence of the random search method in the extremal control of a many parameter system. *Automation & Remote Control*, 24:1337–1342, 1963.
- [42] G. Schrack and M. Choit. Optimized relative step size random searches. *Mathematical Programming*, 10:230–244, 1976.
- [43] M. Schumer and K. Steiglitz. Adaptive step size random search. *IEEE Transactions on Automatic Control*, 13(3):270–276, 1968.
- [44] M. Seungyong, A. Gaon, and O. S. Hyun. Parsimonious black-box adversarial attacks via efficient combinatorial optimization. In *ICML*, 2019.
- [45] S. N. Shukla, A. K. Sahu, D. Willmott, and Z. Kolter. Black-box adversarial attacks with Bayesian optimization. *arXiv preprint arXiv:1909.13857*, 2019.
- [46] J. Su, D. V. Vargas, and K. Sakurai. One pixel attack for fooling deep neural networks. *IEEE Transactions on Evolutionary Computation*, 2019.
- [47] F. Tramr and D. Boneh. Adversarial training and robustness for multiple perturbations. In *NeurIPS*, 2019.
- [48] D. Tsipras, S. Santurkar, L. Engstrom, A. Turner, and A. Madry. Robustness may be at odds with accuracy. *ICLR*, 2019.
- [49] C.-C. Tu, P. Ting, P.-Y. Chen, S. Liu, H. Zhang, J. Yi, C.-J. Hsieh, and S.-M. Cheng. Autozoom: Autoencoder-based zeroth order optimization method for attacking black-box neural networks. In *AAAI Conference on Artificial Intelligence*, 2019.
- [50] J. Uesato, B. O’Donoghue, A. Van den Oord, and P. Kohli. Adversarial risk and the dangers of evaluating against weak attacks. In *ICML*, 2018.
- [51] Z. Yan, Y. Guo, and C. Zhang. Subspace attack: Exploiting promising subspaces for query-efficient black-box attacks. In *NeurIPS*, 2019.
- [52] D. Yin, R. G. Lopes, J. Shlens, E. D. Cubuk, and J. Gilmer. A Fourier perspective on model robustness in computer vision. In *NeurIPS*, 2019.
- [53] S. Zheng, Y. Song, T. Leung, and I. J. Goodfellow. Improving the robustness of deep neural networks via stability training. In *CVPR*, 2016.
- [54] T. Zheng, C. Chen, and K. Ren. Distributionally adversarial attack. In *AAAI*, 2019.

# Supplementary Material

## Organization of the Supplementary Material

In Section A, we present the missing proofs of Section 3 and Section 4 and slightly deepen our theoretical insights on the efficiency of the proposed  $l_\infty$ -attack. Section B covers various implementation details and the hyperparameters we used. In Section C, we discuss the transferability properties of the adversarial examples generated by our attack. We show an ablation study on different choices of the attack's algorithm in Section D. Section E presents the success rate on ImageNet for different number of queries, and also the query efficiency on the challenging models (logit pairing and adversarial training). Finally, since the Square Attack is a randomized algorithm, we show the variance of the main reported performance measures for different random seeds in Section F.

## A. Proofs omitted from Section 3 and Section 4

In this section, we present the proofs omitted from Section 3 and Section 4.

### A.1. Proof of Proposition 3.1

Let  $\delta$  be the output of Algorithm 3. We prove here that  $\|\hat{x} + \delta - x\|_2 = \epsilon$ .

From Step 13 of Algorithm 3, we directly have the equality  $\|\hat{x} + \delta - x\|_2 = \|\nu\|_2$ . Let  $\nu^{\text{old}}$  be the update at the previous iteration, defined in Step 1 and  $\overline{W_1 \cup W_2}$  the indices not belonging to  $W_1 \cup W_2$ . Then,

$$\begin{aligned} \|\nu\|_2^2 &= \sum_{i=1}^c \|\nu_{W_1 \cup W_2, i}\|_2^2 + \sum_{i=1}^c \|\nu_{\overline{W_1 \cup W_2}, i}\|_2^2 \\ &= \sum_{i=1}^c \|\nu_{W_1, i}\|_2^2 + \sum_{i=1}^c \|\nu_{\overline{W_1 \cup W_2}, i}\|_2^2 \\ &= \sum_{i=1}^c (\epsilon_{\text{avail}}^i)^2 + \sum_{i=1}^c \|\nu_{\overline{W_1 \cup W_2}, i}\|_2^2 \\ &= \sum_{i=1}^c \|\nu_{W_1 \cup W_2, i}^{\text{old}}\|_2^2 + \epsilon_{\text{unused}}^2 + \sum_{i=1}^c \|\nu_{\overline{W_1 \cup W_2}, i}\|_2^2 \\ &\stackrel{(i)}{=} \sum_{i=1}^c \|\nu_{W_1 \cup W_2, i}^{\text{old}}\|_2^2 + \epsilon_{\text{unused}}^2 + \sum_{i=1}^c \|\nu_{\overline{W_1 \cup W_2}, i}^{\text{old}}\|_2^2 \\ &= \|\nu^{\text{old}}\|_2^2 + \epsilon_{\text{unused}}^2 \stackrel{(ii)}{=} \epsilon^2, \end{aligned}$$

where (i) holds since  $\nu_{\overline{W_1 \cup W_2}}^{\text{old}} \equiv \nu_{\overline{W_1 \cup W_2}}$  as the modifications affect only the elements in the two windows, and (ii) holds by the definition of  $\epsilon_{\text{unused}}$  in Step 4 of Algorithm 3.

### A.2. Proof of Proposition 4.1

Using the  $L$ -smoothness of the function  $g$ , that is it holds for all  $x, y \in \mathbb{R}^d$ ,

$$\|\nabla g(x) - \nabla g(y)\|_2 \leq L \|x - y\|_2.$$

we obtain (see e.g. [8]):

$$g(x_t + \delta_t) \leq g(x_t) + \langle \nabla g(x_t), \delta_t \rangle + \frac{L}{2} \|\delta_t\|_2^2,$$

and by definition of  $x_{t+1}$  we have

$$\begin{aligned} g(x_{t+1}) &\leq \min\{g(x_t), g(x_t + \delta_t)\} \\ &\leq g(x_t) + \min\{0, \langle \nabla g(x_t), \delta_t \rangle + \frac{L}{2} \|\delta_t\|_2^2\}. \end{aligned}$$

Using the definition of the min as a function of the absolute value ( $2 \min\{a, b\} = a + b - |a - b|$ ) yields

$$\begin{aligned} g(x_{t+1}) &\leq g(x_t) + \frac{1}{2} \langle \nabla g(x_t), \delta_t \rangle + \frac{L}{4} \|\delta_t\|_2^2 \\ &\quad - \frac{1}{2} |\langle \nabla g(x_t), \delta_t \rangle + \frac{L}{2} \|\delta_t\|_2^2|. \end{aligned}$$

And using the triangular inequality ( $|a + b| \geq |a| - |b|$ ), we have

$$\begin{aligned} g(x_{t+1}) &\leq g(x_t) + \frac{1}{2} \langle \nabla g(x_t), \delta_t \rangle + \frac{L}{2} \|\delta_t\|_2^2 \\ &\quad - \frac{1}{2} |\langle \nabla g(x_t), \delta_t \rangle|. \end{aligned}$$

Therefore taking the expectation and using that  $\mathbb{E}\delta_t = 0$ , we get

$$\mathbb{E}g(x_{t+1}) \leq \mathbb{E}g(x_t) - \frac{1}{2} \mathbb{E}|\langle \nabla g(x_t), \delta_t \rangle| + \frac{L}{2} \mathbb{E}\|\delta_t\|_2^2.$$

Therefore, together with Assumption 3 this yields to

$$\mathbb{E}g(x_{t+1}) \leq \mathbb{E}g(x_t) - \frac{\tilde{C}\gamma_t}{2} \mathbb{E}\|\nabla g(x_t)\|_2 + \frac{LC\gamma_t^2}{2},$$

and thus

$$\mathbb{E}\|\nabla g(x_t)\|_2 \leq \frac{2}{\gamma_t \tilde{C}} \left( \mathbb{E}g(x_t) - \mathbb{E}g(x_{t+1}) + \frac{LC\gamma_t^2}{2} \right).$$

Thus for  $\gamma_t = \gamma$  we have summing for  $t = 1 : T$

$$\begin{aligned} \min_{0 \leq i \leq T} \mathbb{E}\|\nabla g(x_i)\|_2 &\leq \frac{1}{T} \sum_{t=0}^T \mathbb{E}\|\nabla g(x_t)\|_2 \\ &\leq \frac{2}{\tilde{C}\gamma T} \left[ g(x_0) - \mathbb{E}g(x_{T+1}) + \frac{TLC\gamma^2}{2} \right]. \end{aligned}$$

We conclude setting the step-size to  $\gamma = \Theta(1/\sqrt{T})$ .

### A.3. Assumption 3 does not hold for the sampling distribution $P$

Let us consider an update  $\delta$  with a window size  $h = 2$  and the direction  $v \in \{-1, 1\}^{w \times w \times c}$  defined as

$$v_{k,l}^i = (-1)^{kl} \quad \text{for all } i, k, l.$$

It is easy to check that any update  $\delta$  drawn from the sampling distribution  $P$  is orthogonal to this direction  $v$ :

$$\langle v, \delta \rangle = \sum_{i=1}^c \sum_{k=r+1}^{r+2} \sum_{l=s+1}^{s+2} (-1)^{kl} = c(-1 + 1 - 1 + 1) = 0.$$

Therefore  $\mathbb{E}|\langle v, \delta \rangle| = 0$  and Assumption 3 does not hold. This implies that the convergence analysis does not directly hold for the sampling distribution  $P$ .

### A.4. Assumption 3 holds for the sampling distribution $P^{\text{multiple}}$

Let us consider the sampling distribution  $P^{\text{multiple}}$  where different Rademacher  $\rho_{k,l,i}$  are drawn for each pixel of the update window  $\delta_{r+1:r+h, s+1:s+h, i}$ . We present it in Algorithm 4 with the convention that any subscript  $k > w$  should be understood as  $k - w$ . This technical modification is greatly helpful to avoid side effect.

Let  $v \in \mathbb{R}^{w \times w \times c}$  for which we have using the Khintchine inequality [24]:

$$\begin{aligned} \mathbb{E}|\langle \delta, v \rangle| &= \mathbb{E} \left| \sum_{k=r+1}^{r+h} \sum_{l=s+1}^{s+h} \sum_{i=1}^c \delta_{k,l}^i v_{k,l}^i \right| \\ &\stackrel{(i)}{=} \mathbb{E}_{(r,s)} \mathbb{E}_{\rho} \left| \sum_{k=r+1}^{r+h} \sum_{l=s+1}^{s+h} \sum_{i=1}^c \delta_{k,l}^i v_{k,l}^i \right| \\ &\stackrel{(ii)}{\geq} \frac{2\varepsilon}{\sqrt{2}} \mathbb{E}_{(r,s)} \|V_{(r,s)}\|_2 \\ &\stackrel{(iii)}{\geq} \sqrt{2}\varepsilon \|\mathbb{E}_{(r,s)} V_{(r,s)}\|_2 \\ &\geq \frac{\sqrt{2}\varepsilon h^2}{w^2} \|v\|_2, \end{aligned}$$

---

**Algorithm 4:** Sampling distribution  $P^{\text{multiple}}$  for  $l_\infty$ -norm

---

- Input:** maximal norm  $\varepsilon$ , window size  $h$ , image size  $w$ , color channels  $c$   
**Output:** New update  $\delta$
- 1  $\delta \leftarrow$  array of zeros of size  $w \times w \times c$
  - 2 sample uniformly  $r, s \in \{0, \dots, w\} \subset \mathbb{N}$
  - 3 **for**  $i = 1, \dots, c$  **do**
  - 4      $\delta_{r+1:r+h, s+1:s+h, i} \leftarrow \text{Uniform}(\{-2\varepsilon, 2\varepsilon\}^{h \times h})$
  - 5 **end**
- 

where we define by  $V_{(r,s)} = \{v_{k,l}^i\}_{k \in \{r+1, \dots, r+h\}, l \in \{s+1, \dots, s+h\}, i \in \{1, \dots, c\}}$  and (i) follows from the decomposition between the randomness of the Rademacher and the random window, (ii) follows from the Khintchine inequality and (iii) follows from Jensen inequality.

In addition we have for the variance:

$$\begin{aligned} \mathbb{E}\|\delta\|_2^2 &= \mathbb{E}_{(r,s)} \sum_{k=r+1}^{r+h} \sum_{l=s+1}^{s+h} \sum_{i=1}^c \mathbb{E}_{\rho} (\delta_{k,l}^i)^2 \\ &= \mathbb{E}_{(r,s)} \sum_{k=r+1}^{r+h} \sum_{l=s+1}^{s+h} \sum_{i=1}^c 4\varepsilon^2 \\ &= 4c\varepsilon^2 h^2. \end{aligned}$$

Thus Assumption 3 holds for the sampling distribution  $P^{\text{multiple}}$ .

### A.5. Why updates of equal sign?

Proposition 4.1 underlines the importance of a large inner product  $\mathbb{E}[\langle \delta_t, \nabla g(x_t) \rangle]$  in the direction of the gradients. This provides some intuition explaining why the update  $\delta^{\text{single}}$  where a single Rademacher is drawn for each window  $\delta_{r+1:r+h, s+1:s+h, i}$  is more efficient than the update  $\delta^{\text{multiple}}$  where different Rademacher are drawn. Following the observation that adversarial gradients are often piecewise constant [26] we consider, as a heuristic, a piecewise constant direction  $v$  for which

$$\mathbb{E}[\langle \delta^{\text{single}}, v \rangle] = O(\|v\|_1) \quad \text{and} \quad \mathbb{E}[\langle \delta^{\text{multiple}}, v \rangle] = O(\|v\|_2).$$

Therefore the directions sampled by our proposal are more correlated with the gradient direction and help the algorithm to converge faster. This is also verified empirically in our experiments (see the ablation study in Sup. D).

**Analysis.** Let us consider the direction  $v \in \mathbb{R}^{w \times w}$  composed of different blocks  $\{V_{(r,s)}\}_{(r,s) \in \{0, \dots, w/h\}}$  of constant sign.

For this direction  $v$  we compare two different proposal  $P^{\text{multiple}}$  and  $P^{\text{single}}$  where we choose uniformly one random block  $(r, s)$  and we either assign a single Rademacher  $\rho_{(r,s)}$  to the whole block (this is  $P^{\text{single}}$ ) or we assign multiple Rademacher  $\{\rho_{(k,l)}\}_{k \in \{rh+1, \dots, (r+1)h\}, l \in \{sh+1, \dots, (s+1)h\}}$  (this is  $P^{\text{multiple}}$ ). We have

$$\begin{aligned} \mathbb{E}|\langle \delta^{\text{multiple}}, v \rangle| &= \mathbb{E} \left| \sum_{k=rh+1}^{(r+1)h} \sum_{l=sh+1}^{(s+1)h} \delta_{k,l} v_{k,l} \right| \\ &\geq \frac{2\varepsilon}{\sqrt{2}} \mathbb{E}_{(r,s)} \|V_{(r,s)}\|_2 \\ &\geq \frac{\sqrt{2}\varepsilon h^2}{w^2} \sum_{r=1}^{w/h} \sum_{s=1}^{w/h} \|V_{(r,s)}\|_2. \end{aligned}$$

Therefore we obtain the  $l_1/l_2$ -norm of the different groups. For the update  $\delta^{\text{single}}$  we obtain

$$\begin{aligned} \mathbb{E}|\langle \delta^{\text{single}}, v \rangle| &= \mathbb{E} \left| \sum_{k=rh+1}^{(r+1)h} \sum_{l=sh+1}^{(s+1)h} \delta_{r,s} v_{k,l} \right| \\ &= \mathbb{E} |\delta_{r,s} \sum_{k=rh+1}^{(r+1)h} \sum_{l=sh+1}^{(s+1)h} v_{k,l}| \\ &\stackrel{(i)}{=} 2\varepsilon \mathbb{E}_{(r,s)} \|V_{(r,s)}\|_1 \\ &= \frac{2\varepsilon h^2}{w^2} \|v\|_1 \end{aligned}$$

where (i) follows from the fact the  $V_{(r,s)}$  has a constant sign. We recover then the  $l_1$ -norm of the direction  $v$ .

For quasi-constant block, then  $\mathbb{E}|\langle \delta^{\text{single}}, v \rangle|$  will be larger than  $\mathbb{E}|\langle \delta^{\text{multiple}}, v \rangle|$ . For instance, in the extreme case of constant binary block  $|V_{(r,s)}| = 11^\top$ , we have

$$\mathbb{E}|\langle \delta^{\text{single}}, v \rangle| = 2\varepsilon h^2 \gg \mathbb{E}|\langle \delta^{\text{multiple}}, v \rangle| = 2\varepsilon h.$$

## A.6. Proof of Proposition 4.2

Let  $x \in \mathcal{F}$ , and  $N(x)$  the number of elements of  $\mathcal{G}$  that  $x$  contains. Let initialize  $x$  as a square of size  $s \times s$ , so that  $N(x) = 1$ . We then add iteratively the remaining  $k - s^2$  unitary squares to  $x$  so to maximize  $N(x)$ .

In order to get  $N(x) = 2$  it is necessary to increase  $x$  to have size  $s \times (s + 1)$ . At this point, again to get  $N(x) = 3$  we need to add  $s$  squares to one side of  $x$ . However, if we choose to glue them so to form a rectangle  $s \times (s + 2)$ , then  $N(x) = 3$  and once more we need other  $s$  squares to increase  $N$ , which means overall  $s^2 + 3s$  to achieve  $N(x) = 4$ . If instead we glue  $s$  squares along the longer side, with only one additional unitary square we get  $N(x) = 4$  using  $s^2 + 2s + 1 < s^2 + 3s$  unitary squares (as  $s \geq 2$ ), with  $x = (s + 1) \times (s + 1)$ .

Then, if the current shape of  $x$  is  $a \times b$  with  $a \geq b$ , the optimal option is adding  $a$  unitary squares to have shape  $a \times (b + 1)$ , increasing the count  $N$  of  $a - s + 1$ . This strategy can be repeated until the budget of  $k$  unitary squares is reached. Finally, since we start from the shape  $s \times s$ , then at each stage  $b - a \in \{0, 1\}$ , which means that the final  $a$  will be  $\lfloor \sqrt{k} \rfloor$ . A rectangle  $a \times b$  in  $\mathcal{F}$  contains  $(a - s + 1)(b - s + 1)$  elements of  $\mathcal{G}$ . The remaining  $k - ab$  squares can be glued along the longer side, contributing to  $N(x)$  with  $(k - ab - s + 1)^+$ .

## B. Experimental details

In this section, we list the main hyperparameters and various implementation details.

### B.1. Experiments on ImageNet

For the Square Attack on the ImageNet models, we used  $p = 0.05$  and  $p = 0.1$  for the  $l_\infty$  and  $l_2$  versions respectively. For Bandits, we used their code with their suggested hyperparameters (specified in the configuration files) for both  $l_\infty$  and  $l_2$ . For SimBA-DCT, we used the default parameters of the original code apart from the following, which are the suggested ones for each model: for ResNet-50 and VGG-16-BN “freq\_dims” = 28, “order” = “strided” and “stride” = 7, for Inception v3 “freq\_dims” = 38, “order” = “strided” and “stride” = 9. The results for all other methods were taken directly from the corresponding papers.

**Evaluation of Bandits.** The code of Bandits [26] does not have image standardization at the stage where the set of correctly points is determined (see <https://github.com/MadryLab/blackbox-bandits/issues/3>). As a result, the attack is run only on the set of points correctly classified by the network *without standardization*, although the network was trained on standardized images. We fix this bug, and report the results in Table 1 based on the fixed version of their code. We note that the largest difference of our evaluation compared to the  $l_\infty$  results reported in Appendix E of [26] is obtained for the VGG-16-BN network: we get 2.0% failure rate while they reported 8.4% in their paper. Also, we note that the query count for Inception v3 we obtain is also better than reported in [26]: 957 instead of 1117 with a slightly better failure rate. Our  $l_2$  results also differ – we obtain a significantly lower failure rate (9.8%, 6.8%, 10.2% instead of 15.5%, 9.7%, 17.2% for the Inception v3, ResNet-50, VGG-16-BN networks respectively) with improved average number of queries (1486, 939, 511 instead of 1858, 993, 594).

### B.2. Experiments on challenging tasks

For the  $l_\infty$  Square Attack, we used  $p = 0.3$  for all models on MNIST, CIFAR-10, and also on the post-averaging model [30] on ImageNet. For Bandits on MNIST and CIFAR-10 adversarially trained models we used “exploration” = 0.1, “tile size” = 16, “gradient iters” = 1 following [44].

For the comparison of  $l_2$  attacks on the  $l_\infty$  adversarially trained model of [31] we used the Square Attack with the usual parameter  $p = 0.1$ . For Bandits we used the parameters “exploration” = 0.01, “tile size” = 28, “gradient iters” = 1, after running a grid search over the three of them (all the other parameters are kept as set in the original code). For SimBA we used the “pixel attack” with parameters “order” = “rand”, “freq\_dims” = 28, step size of 0.50, after a grid search on all the parameters.

## C. Transferability experiment

We study the transferability properties of the adversarial examples generated by the Square Attack on three standardly trained models: DenseNet-121, ResNet-50, and VGG-16-BN. Note that we additionally use a DenseNet-121 model (also from PyTorch repository) instead of Inception v3 to make all models use the same input size ( $224 \times 224 \times 3$ ). In Table 7, we report for this model the failure rate and query efficiency, which are close to the results of ResNet-50 reported in Table 1 and prove again that our failure rate and the required number of queries are very low.

Norm	$\epsilon$	Failure rate	Avg. queries	Median queries
$l_\infty$	0.05	0.0%	64	13
$l_2$	5	0.9%	519	150

Table 7. Results for the DenseNet-121 model on ImageNet which is used as an additional model in the transferability experiments.

We additionally evaluate the PGD attack in order to have a comparison to a standard white-box attack. For both the Square and PGD attacks, we generate *untargeted* adversarial examples for the source models, and then evaluate the two other target models on them. As before, we generate adversarial examples only on the points that were initially correctly classified. Unlike in the previous experiments, here we generate *high-confidence* adversarial examples, i.e. we stop the optimization procedure in the attacks only when the predicted confidence in a wrong class reaches 95%, and we filter out the examples for which we cannot achieve this level of confidence within 10,000 queries. Similarly, also for PGD we consider only adversarial perturbations which achieve such high confidence.

The results are shown in Tables 8 and 9, where an untargeted success means any misclassification, and a targeted success means a misclassification to the same wrong class predicted by the source model. We report both metrics since they capture different aspects of the transferability phenomenon. Note that by construction the transfer rate is 100% if the source model is equal to the target model (this is why there is 100% on the diagonal in each table).

First, we note that our  $l_\infty$ - and  $l_2$ -attacks have much lower targeted transferability rates than the PGD attack. For example, the targeted transferability rate for the  $l_2$ -perturbations from DenseNet to ResNet is very low for the Square Attack (10.1%), while it is quite significant for PGD (47.8%). The untargeted transferability rates are also considerably lower for the  $l_2$  Square Attack compared to the PGD attack, in average by a factor of 3. The untargeted transferability for the  $l_\infty$  Square Attack is similar to PGD. Finally, we note that the transferability rates for the  $l_2$  Square Attack are in average considerably lower than for

a) Targeted transferability (Square Attack / PGD)			
Source	Target models		
	DenseNet	ResNet	VGG
DenseNet	100% / 100%	21.0% / 51.5%	20.3% / 41.3%
ResNet	19.1% / 43.4%	100% / 100%	23.8% / 35.8%
VGG	13.2% / 16.2%	10.4% / 16.9%	100% / 100%

b) Untargeted transferability (Square Attack / PGD)			
Source	Target models		
	DenseNet	ResNet	VGG
DenseNet	100% / 100%	46.8% / 68.3%	60.5% / 61.3%
ResNet	43.9% / 55.2%	100% / 100%	58.9% / 53.6%
VGG	37.0% / 31.0%	39.2% / 31.1%	100% / 100%

Table 8. Transferability success rate of  $l_\infty$  ( $\epsilon = 0.05$ ) Square / PGD attacks generated with high confidence (at least 95%). **a)** Targeted and **b)** Untargeted attacks transferability rates on standardly trained DenseNet-121, ResNet-50, VGG-16-BN models.

a) Targeted transferability (Square Attack / PGD)			
Source	Target models		
	DenseNet	ResNet	VGG
DenseNet	100% / 100%	10.1% / 47.8%	11.8% / 42.8%
ResNet	11.1% / 41.6%	100% / 100%	10.6% / 38.5%
VGG	6.8% / 9.7%	6.8% / 10.6%	100% / 100%

b) Untargeted transferability (Square Attack / PGD)			
Source	Target models		
	DenseNet	ResNet	VGG
DenseNet	100% / 100%	15.4% / 63.0%	18.2% / 61.2%
ResNet	17.4% / 52.8%	100% / 100%	18.0% / 55.8%
VGG	13.4% / 21.7%	11.9% / 25.3%	100% / 100%

Table 9. Transferability success rate of  $l_2$  ( $\epsilon = 5$ ) Square / PGD attacks generated with high confidence (at least 95%). **a)** Targeted and **b)** Untargeted attacks transferability rates on standardly trained DenseNet-121, ResNet-50, VGG-16-BN models.

the  $l_\infty$  Square Attack, while for PGD there is no significant difference in transferability between the two norms.

This shows that adversarial examples generated in a different way, i.e. without using any gradient information, can have quite different properties (e.g. transferability), compared to usual gradient-based adversarial examples.

## D. Ablation study

Here we discuss the results of an ablation study which justifies the algorithmic choices made for the Square Attack. Additionally, we discuss the robustness of the attack to the hyperparameter  $p$ , i.e. the initial fraction of pixels changed by the attack (see Figure 4). We perform all these experiments on ImageNet with a standardly trained ResNet-50 model from the PyTorch repository.

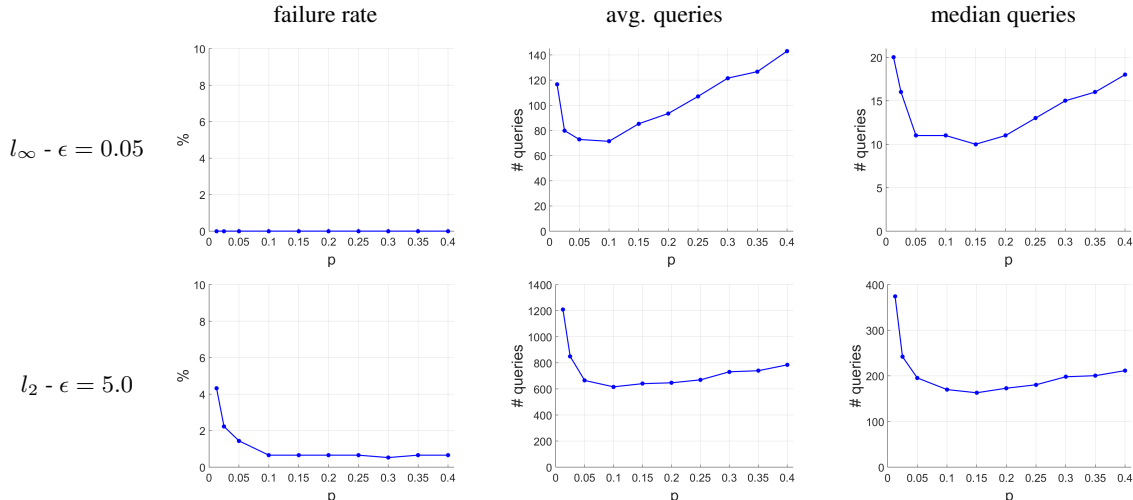


Figure 4. Sensitivity of the Square Attack to different choices of  $p \in \{0.0125, 0.025, 0.05, 0.1, 0.15, 0.2, 0.25, 0.3, 0.35, 0.4\}$ , i.e. the initial fraction of pixels changed by the attack, on ImageNet for a ResNet-50 model.

### D.1. $l_\infty$ Square Attack

**Sensitivity to the hyperparameter  $p$ .** First of all, we note that for *all* values of  $p$  we achieve 0.0% failure rate. Moreover, we achieve state-of-the-art query efficiency with *all* considered values of  $p$  (from 0.0125 to 0.4), i.e. we have the mean number of queries below 140, and the median below 20 queries. Therefore, we conclude that the attack is robust to a wide range of  $p$ , which is an important property of a black-box attack – since the target model is unknown, and one aims at minimizing the number of queries needed to fool the model, doing even an approximate grid search over  $p$  is prohibitively expensive.

**Algorithmic choices.** In Table 10, we analyze the influence of different algorithmic choices on the performance of the  $l_\infty$  Square Attack, in particular the type of the update  $\delta$  and the initialization scheme. First, we note that the failure rate is 0% for all models, i.e. the random search scheme is always able to find adversarial examples for every image, even with suboptimal choices of the sampling distribution or suboptimal initialization. Also, note that most of the considered configurations still lead to the state-of-the-art query efficiency. Importantly, having square-shaped updates (see column “Update shape”) is indeed crucial – it leads to 5 $\times$  better query efficiency (both in terms of the mean and median) compared to changing a fraction of  $p$  random pixels for every update (number of pixels changed is the same as for squares).

Another important idea that leads to 2 $\times$  better query efficiency is to use the same random signs across different locations. We elaborated on the importance of this algorithmic choice in Sec. A.5, and here we confirm the finding experimentally. Column “# random signs” in Table 10 cor-

responds to the number of random signs sampled for every update  $\delta$  (for a single image). Note that the best performing scheme (as described in Algorithm 2) is to have the same sign of the update at every location of the square, but different sign for every color channel. Thus, this corresponds to  $c$  random signs, assuming that there are  $c$  color channels. An alternative is to use the same random sign also for all color channels, which leads to only 1 random sign, but this scheme performs 1.5 $\times$  worse in terms of the mean and median number of queries. Even worse is choosing the sign randomly for all pixels and color channels (denoted as  $c \cdot h^2$ , where  $h$  is the size of the square).

Finally, we can see that the initialization with vertical stripes helps to significantly improve the query efficiency (particularly, the median) compared to other initialization methods, such as horizontal stripes, randomly placed squares or uniformly random initialization  $\delta \in Uniform(\{-\epsilon, \epsilon\}^d)$ .

### D.2. $l_2$ Square Attack

**Sensitivity to the hyperparameter  $p$ .** The  $l_2$  Square Attack is robust to different choices in the range between 0.05 and 0.4 showing approximately the same failure rate and query efficiency for all values of  $p$  in this range, while its performance degrades slightly for very small initial squares  $p \in \{0.0125, 0.025\}$ .

**Algorithmic choices.** We analyze in Table 10 the sensitivity of the  $l_2$  attack to different choices of the shape of the update added at each iteration and initialization.

In particular, we test an update with only one “center” instead of two, namely  $\eta^{\text{single}} = \eta^{h,h}$  (following the notation of Eq. 2) and one,  $\eta^{\text{rand}}$ , where the step 7 in Al-

Update shape	# random signs	Initialization	Failure rate	Avg. queries	Median queries
random	$c \cdot h^2$	vert. stripes	0.0%	401	48
random	$c$	vert. stripes	0.0%	339	53
square	$c \cdot h^2$	vert. stripes	0.0%	153	15
square	1	vert. stripes	0.0%	129	18
square	$c$	uniform rand.	0.0%	91	26
square	$c$	rand. squares	0.0%	90	20
square	$c$	horiz. stripes	0.0%	83	18
square	$c$	vert. stripes	0.0%	73	11

Update	Initialization	Failure rate	Avg. queries	Median queries
$\eta^{\text{rand}}$	$\eta^{\text{rand}}\text{-grid}$	3.3%	1050	324
$\eta^{\text{single}}$	$\eta^{\text{single}}\text{-grid}$	0.7%	650	171
$\eta$	gaussian	0.4%	696	189
$\eta$	uniform	0.8%	660	187
$\eta$	vert. stripes	0.8%	655	186
$\eta$	$\eta\text{-grid}$	0.7%	616	170

Table 10. An ablation study for the performance of the  $l_\infty$  and  $l_2$  Square Attack under various algorithmic choices of the attack. The statistics are calculate on 1,000 ImageNet images for a ResNet-50 model. The last row represents our recommended setting used in Sec. 5.1. For all experiments we used the best performing  $p$  (0.05 for  $l_\infty$  and 0.1 for  $l_2$ ).

gorithm 3 is  $\rho \leftarrow \text{Uniform}(\{-1, 1\}^{h \times h})$  instead of  $\rho \leftarrow \text{Uniform}(\{-1, 1\})$ , which means that each element of  $\eta$  is multiplied randomly by either  $-1$  or  $1$  independently (instead of all elements multiplied by the same value). We can see that using different random signs in the update ( $\eta^{\text{rand}}$ ) significantly ( $1.5 \times$  factor) degrades the results for the  $l_2$  attack, which is similar to the observation made for the  $l_\infty$  attack.

Alternatively to the grid described in Sec. 3.4, we consider as starting perturbation i) a random point sampled according to  $\text{Uniform}(\{-\epsilon/\sqrt{d}, \epsilon/\sqrt{d}\}^{w \times w \times c})$ , that is on the corners of the largest  $l_\infty$ -ball contained in the  $l_2$ -ball of radius  $\epsilon$  (uniform initialization), ii) a random position on the  $l_2$ -ball of radius  $\epsilon$  (gaussian initialization) or iii) vertical stripes similarly to what done for the  $l_\infty$  Square Attack, but with magnitude  $\epsilon/\sqrt{d}$  to fulfill the constraints on the  $l_2$ -norm of the perturbation. We note that different initialization schemes do not have a large influence on the results of our  $l_2$  attack, unlike for the  $l_\infty$  attack (the slightly better success rate achieved with Gaussian initialization is most likely due to the random component of random search rather than to an effective superiority of such initialization). Then our  $l_2$  attack is able to effectively move the mass of the perturbation where it is necessary to achieve a misclassification without relying on a particular starting distribution.

## E. Additional experimental results

This section contains additional experimental results that complement the ImageNet results from Table 1, and the results on challenging models from Tables 4, 5, 6.

### E.1. Success rate on ImageNet for different number of queries

In this section, we provide a more detailed comparison to the competitors from Table 1 under different query budget. We make an additional comparison to BayesAttack of [45] which achieves a state-of-the-art success rate in the *low query regime*, which is defined in [45] as a regime when the attacker has only up to 200 queries (unlike 10,000 queries commonly reported in the literature) to create an adversarial example. In particular, they outperform all recently proposed black-box attacks [44, 34, 26] in this setting.

We show in Figure 5 the behaviour of the success rate for each attack depending on the number queries. The success rates of the attacks from [34] (DFO<sub>c</sub> – CMA – 50 and DFO<sub>d</sub> – Diag. CMA – 30) and [45] (BayesAttack) for different number of queries were obtained via personal communication directly from the authors, and were calculated on 500 and 10,000 randomly sampled points, respectively. Our results, as before, were calculated on 1,000 randomly sampled points.

**$l_\infty$  results:** First, we observe that the Square Attack outperforms all other methods in the standard regime with 10,000 queries. The gap in the success rate is particularly large in the range of 100 – 1000 queries. In particular, our method also outperforms the BayesAttack in the low query regime by approximately 20% on every model, thus achieving a new state-of-the-art success rate in this regime. We note that DFO<sub>d</sub> – Diag. CMA – 30 method is also quite effective in the low query regime showing results close to BayesAttack. However, it is also outperformed by our Square Attack.

**$l_2$  results:** The  $l_2$  Square Attack outperforms both Bandits and SimBA, and the gap is particularly large in the low query regime. We note that the success rate of SimBA plateaus after some iteration. This happens due to the fact that their algorithm only adds orthogonal updates to the perturbation, and does not have any way to correct the greedy decisions made earlier. Thus, there is no progress anymore after the norm of the perturbation reaches the  $\epsilon = 5$  (note that we used for SimBA the same parameters of the comparison between SimBA and Bandits in [23]). Contrary to this, both Bandits and our attack constantly keep improving the success rate, although with a different speed.

### E.2. Query efficiency on challenging tasks

**$l_\infty$  experiments** We compare additionally the query efficiency of the Square Attack versus Bandits [26] in Table 11.



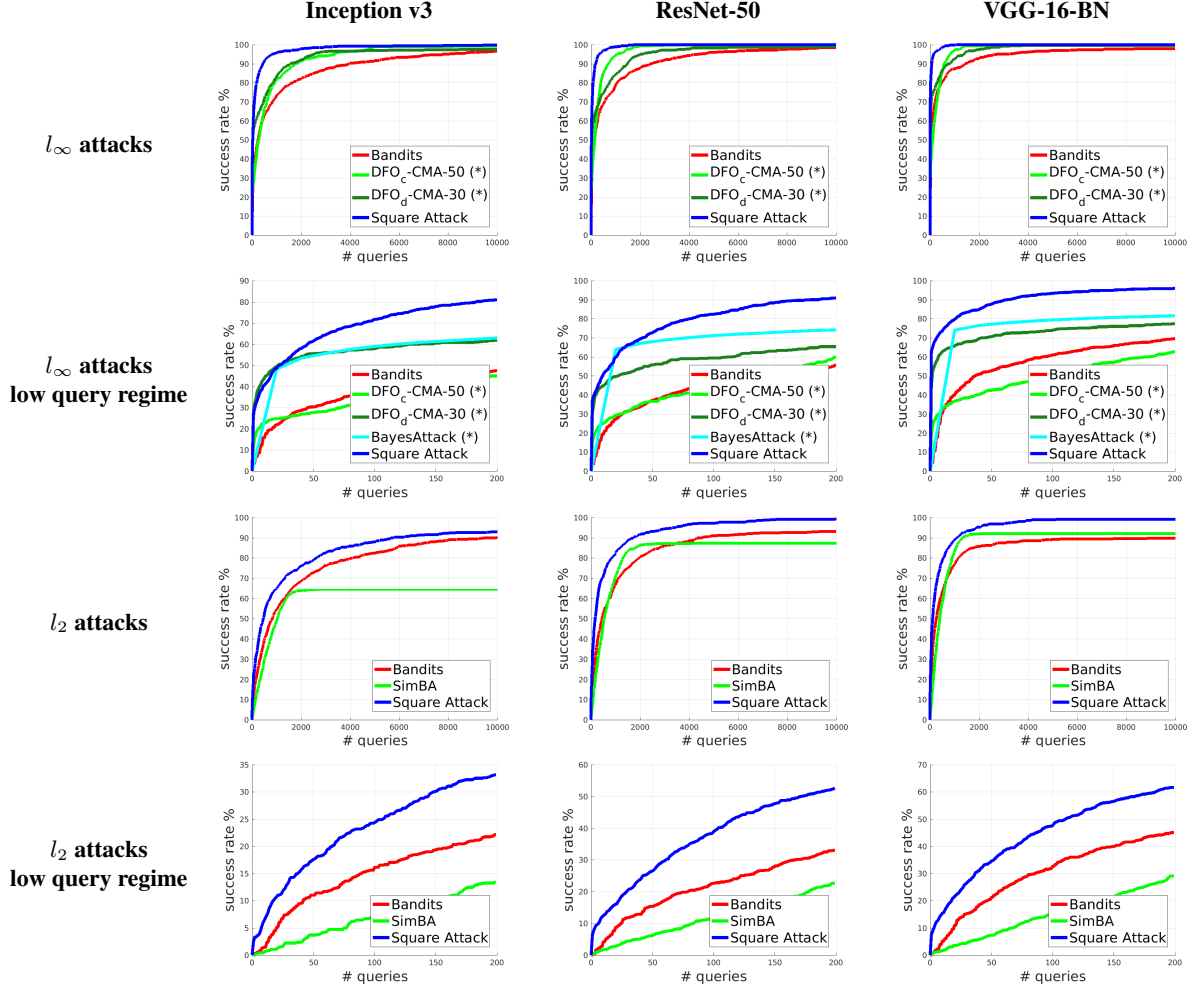


Figure 5. Success rate vs number of queries for different attacks on ImageNet on three standardly trained models. The low query regime corresponds to up to 200 queries, while the standard regime corresponds to 10,000 queries. \* denotes the results obtained via personal communication with the authors and evaluated on 500 and 10,000 randomly sampled points for BayesAttack [45] and DFO [34] methods, respectively. Note that for BayesAttack only the success rate every 20 queries is available.

We can observe that there is a significant difference not only in terms of robust accuracy, but also in terms of the mean and median number of queries required to find adversarial examples. On many models the difference in the mean and median number of queries needed for our method is *an order of magnitude less* than for Bandits. For example, only 256 queries are needed on average for  $LSQ_{MNIST}$  model for our method to achieve 2.6% robust accuracy instead of 4137 queries needed for Bandits to achieve 37.3% robust accuracy.

**$l_2$  experiments** We show in Figure 6 the success rate depending on the number of queries used by each of the  $l_2$  attacks on the  $l_\infty$  adversarially trained model of [31] on MNIST, considering 5 thresholds  $\epsilon$  corresponding to the  $l_2$ -norm of the adversarial perturbations ( $\epsilon \in \{1.0, 1.5, 2.0, 2.5, 3.0\}$ ). Note that the maximum number of queries which SimBA uses is  $2 \cdot d$ , where  $d$  is the total

number of pixels, so that for MNIST its results cannot improve after 1568 queries. In practice however SimBA takes many fewer iterations to reach the final results, although we tested different step sizes to mitigate this phenomenon and get a better success rate.

The plots highlight how the Square Attack achieves the highest success rate at all the thresholds  $\epsilon$ , with a large gap compared to Bandits and SimBA especially for the intermediate  $\epsilon$ .

## F. Stability of the attack under different random seeds

Here we study the stability of the Square Attack over the randomness in the algorithm, that is the randomness intrinsic in the initialization, in the choice of the locations of square-shaped regions, and in the choice of the values in the

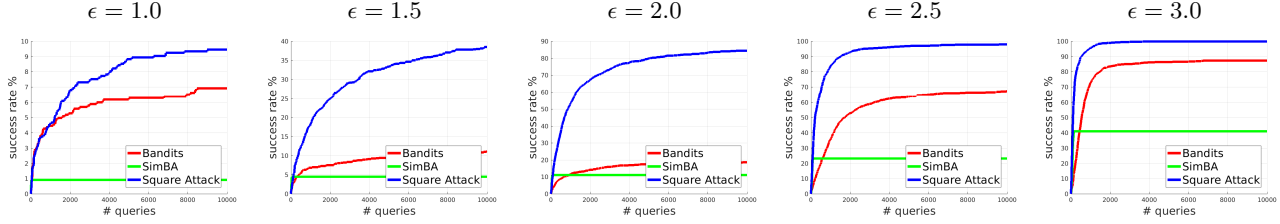


Figure 6. Success rate vs queries of the  $l_2$  attacks on the  $l_\infty$  adversarially trained model of [31] at the different thresholds  $\epsilon$ .

		Square Attack / Bandits		
$\epsilon_\infty$	Model	Robust accuracy	Mean	Median
0.3	CLP <sub>MNIST</sub>	<b>6.1%</b> / 33.3%	<b>378</b> / 3760	<b>53</b> / 1784
0.3	LSQ <sub>MNIST</sub>	<b>2.6%</b> / 37.3%	<b>256</b> / 4137	<b>57</b> / 2308
0.3	AT <sub>MNIST</sub>	<b>87.1%</b> / 89.4%	<b>271</b> / 2128	<b>56</b> / 634
16/255	CLP <sub>CIFAR</sub>	<b>0.2%</b> / 14.3%	<b>240</b> / 1401	<b>30</b> / 1020
16/255	LSQ <sub>CIFAR</sub>	<b>7.2%</b> / 27.7%	<b>684</b> / 3217	<b>33</b> / 1292
8/255	AT <sub>CIFAR</sub>	<b>46.1%</b> / 52.7%	<b>1716</b> / 2725	<b>430</b> / 1615

Table 11.  $l_\infty$  robustness and query efficiency on challenging tasks: Clean Logit Pairing (CLP), Logit Squeezing (LSQ) and Adversarial training (AT). We provide a comparison for the square attack and bandits.

updates  $\delta$ . We repeat the experiments reported in Sec. 5.1 and Sec. 5.2 10 times on 1,000 images using the ResNet-50 on ImageNet and the adversarially trained LeNet on MNIST with different random seeds for the attack. In Table 12, we report the mean and standard deviation of the success rate of our attack, and average and median number of queries needed to find an adversarial example.

On the ImageNet model, all these metrics are very concentrated for both  $l_\infty$ - and  $l_2$ -norms. Thus we conclude that the results of the attack are stable under different random seeds. Moreover, we note that the standard deviations are much smaller than the gap between the Square Attack and the competing methods reported in Table 1.

On the adversarially trained MNIST model, the robust accuracy is very concentrated showing only 0.1% and 1.4% standard deviations for  $l_\infty$ - and  $l_2$ -norms respectively. Importantly, this is much less than the gaps to the nearest competitors reported in Tables 5 and 6. The standard deviation of the mean number of queries is, however, higher than for ImageNet, particularly for our  $l_\infty$ -attack, but the median is still relatively concentrated. This is possibly due to the fact that attacking robust (or not standardly trained models) is a more challenging task than finding adversarial perturbations for plain classifiers (as those used on ImageNet), which means the favorable (random) initialization or sampling can be more influential for the query efficiency.

ImageNet, ResNet-50				
Norm	$\epsilon$	Failure rate	Avg. queries	Median queries
$l_\infty$	0.05	0.0% $\pm$ 0.0%	72 $\pm$ 2	11 $\pm$ 1
$l_2$	5	0.6% $\pm$ 0.1%	638 $\pm$ 12	163 $\pm$ 8

MNIST, adversarially trained LeNet from [31]				
Norm	$\epsilon$	Failure rate	Avg. queries	Median queries
$l_\infty$	0.3	87.0% $\pm$ 0.1%	299 $\pm$ 47	52 $\pm$ 7
$l_2$	2	16.3% $\pm$ 1.4%	1454 $\pm$ 71	742 $\pm$ 78

Table 12. Mean and standard deviation of the main performance metrics of the Square Attack across 10 different runs with different random seeds.